Applied Physics Letters

Generation-recombination and 1/*f* noise in carbon nanotube networks

Cite as: Appl. Phys. Lett. **118**, 242102 (2021); https://doi.org/10.1063/5.0054845
Submitted: 22 April 2021 . Accepted: 26 May 2021 . Published Online: 15 June 2021

A. Rehman, A. Krajewska, B. Stonio, K. Pavlov, G. Cywinski, D. Lioubtchenko, W. Knap, S. Rumyantsev, and J. M. Smulko

AIP Publishing

Applied Physics Letters ARTICLE scitation.org/journal/apl

Generation-recombination and 1/*f* noise in carbon nanotube networks

Cite as: Appl. Phys. Lett. **118**, 242102 (2021); doi: 10.1063/5.0054845
Submitted: 22 April 2021 · Accepted: 26 May 2021 ·
Published Online: 15 June 2021

View Online Export Citation CrossMark

A. Rehman,[1,a)] A. Krajewska,[1] B. Stonio,[1,2] K. Pavlov,[2] G. Cywinski,[1,2] D. Lioubtchenko,[1,3] W. Knap,[1,2,4] S. Rumyantsev,[1] and J. M. Smulko[5]

AFFILIATIONS

[1]CENTERA Laboratories, Institute of High Pressure Physics PAS, Sokołowska 29/37, 01-142 Warsaw, Poland
[2]Centre for Advanced Materials and Technologies CEZAMAT, Warsaw University of Technology, Poleczki 19, 02-822 Warsaw, Poland
[3]Division of Micro and Nanosystems, KTH Royal Institute of Technology, Malvinas Väg 10, SE-100 44 Stockholm, Sweden
[4]Laboratoire Charles Coulomb, University of Montpellier and CNRS UMR 5221, 34950 Montpellier, France
[5]Department of Metrology and Optoelectronics, Faculty of Electronics, Telecommunications, and Informatics, Gdańsk University of Technology, G. Narutowicza 11/12, 80-233 Gdańsk, Poland

[a)]**Author to whom correspondence should be addressed:** adilrehhman@gmail.com

ABSTRACT

The low-frequency noise is of special interest for carbon nanotubes devices, which are building blocks for a variety of sensors, including radio frequency and terahertz detectors. We studied noise in as-fabricated and aged carbon nanotube networks (CNNs) field-effect transistors. Contrary to the majority of previous publications, as-fabricated devices demonstrated the superposition of generation-recombination (GR) and 1/*f* noise spectra at a low-frequency range. Although all the devices revealed identical current–voltage characteristics, GR noise was different for different transistors. This effect is explained by the different properties and concentrations of trap levels responsible for the noise. Unexpectedly, exposure of these devices to the atmosphere reduced both the resistance and GR noise due to nanotube's *p*-doping by adsorbed water molecules from the ambient atmosphere. The presence of the generation recombination noise and its dependences on the environment provides the basis for selective gas sensing based on the noise measurements. Our study reveals the noise properties of CNNs that need to be considered when developing carbon nanotubes-based selective gas sensors.

Distinctive carbon nanotubes (CNs) structure is a unique platform for studying the physics of low-dimensional systems and building electronic devices. There are two major approaches for CN-based devices: one relies on a single nanotube or nanotubes bundles, whereas the second approach is based on the randomly distributed CN networks (CNNs). The main advantage of the second approach is its fabrication simplicity since it does not require a precise manipulation of a single nanotube. It also allows for multiple device production via the standard photolithography technique. The characteristics of devices can easily be adjusted by network density and dimensions. CNNs-based devices compete with silicon thin-film transistors,[1,2] graphene-based elements, and transition metal di-chalcogenides-based transistors, like MoS_2.[3] The exceptional volume to surface ratio of CNNs makes them promising for biological and gas sensing.[4,5] Moreover, CNNs transistors have potential applications in transparent and flexible electronics,[6–8] high frequency, and terahertz devices.[9–11]

The low-frequency (flicker) noise is an essential parameter for almost any electronic device. It is of particular interest for high-frequency applications as it defines the Noise Equivalent Power (NEP) of detectors and phase noise of high-frequency generators and mixers. CNs are promising room temperature THz detectors and other devices.[12] Efficient single detectors and even cameras based on CNs are already demonstrated.[10,11,13] The low-frequency noise in electronic devices is often a superposition of 1/*f* and generation (GR) recombination noise. The 1/*f* noise is evidence of exponentially wide distribution of characteristic times of random processes contributing to the noise, whereas the GR noise indicates an intense random process with just one well-defined time constant, contributing to the overall noise.

Although several studies have already been reported on noise in CNs,[14–21] the nature of the low-frequency noise is still debating. The majority of the publications report only on $1/f^{\gamma}$ noise with the exponent γ close to unity and the amplitude dependent on several factors.

So far, we are aware only of a few studies, where the well-defined GR noise is reported in a single nanotube device.[22,23] Here, we demonstrate that GR noise can contribute significantly to the low-frequency noise in CNNs devices. Though the current–voltage characteristics of the studied devices were the same, noise varied between the specimens from the same batch, owing to different concentrations of trap levels. We further extended the study to aged CNNs-based transistors and explained the results via the absorption of water molecules from the ambient atmosphere on CNNs. These results might play a significant role to understand the behavior of as-fabricated and aged carbon nanotubes-based devices in their perspective applications.

The randomly oriented carbon nanotube networks were synthesized via aerosol chemical vapor deposition method[24] and then transferred on low resistive (<0.005 Ω/cm) oxidized Si substrate by dry transfer method.[25,26] Figures 1(a) and 1(b) show the scanning electron microscope (SEM) images of nanotube networks at different magnifications. The structural morphology reveals low densities of the randomly oriented networks of CNs, which, in turn, reflects their high optical transparency. The contacts in the form of transmission line model (TLM) structures were patterned via electron beam lithography prior to the deposition of CNNs on 170 nm-thick SiO_2 layer. The optical microscope image of the TLM structures with deposited nanotube networks (seen as a slightly darker area) is shown in Fig. 1(c). Each pair of device contacts were used as source and drain terminals of a field-effect transistor with Si substrate acting as a back-gate contact. Schematic view of the back-gated CNNs transistor along with biasing scheme is shown in Fig. 1(d). InVia reflex Renishaw Raman microscope was employed to examine the structural morphology of nanotube networks. Excitation power of the Nd: YAG laser beam (532 nm) was 2.1 mW, which was directed to a sample through 100× objective lens. Raman signal was collected over a wide spectral range of 70–2200 cm^{-1} with 13 s exposition time and single accumulation per measurement.

A low-noise voltage amplifier (Signal Recovery MODEL 5184) was used for noise measurements to amplify the voltage fluctuations measured across the load resistor, R_L. The recorded voltage time series were Fast Fourier Transformed by the "PHOTON" dynamic signal analyzer (Bruel & Kjaer an HBK Company). The estimated voltage noise power spectral density, S_V, was converted into current noise power spectral density, S_I via equation $S_I = S_V(\frac{R_L+R_D}{R_L \times R_D})^2$. Here, R_D is the DC resistance of CNNs device. To evaluate the inherent noise of the system, CNNs device was replaced by the metal resistor of the same DC resistance value as the studied device. The observed background noise of the measurement set-up was at least 20 dB lower than the noise of the tested devices within the analyzed frequency range.

Raman spectroscopy is one of the most effective and nondestructive techniques to characterize the properties of low-dimensional materials, including carbon nanotubes. It allows to estimate the diameter and overall quality of the CNNs.[26–28] Figure 2(a) shows the Raman spectra of the studied nanotube networks. The characteristics peaks that appeared at ∼130, ∼1350, ∼1580, and ∼2680 cm^{-1} are denoted as radial breathing mode (RBM) peak, D-peak, G-peak, and 2D-peak, respectively. These peaks are typical for CNs and among them, RBM and graphitic G-peaks are referred to as the strongest features of CNs Raman spectra.[28–30] Raman D-peak is associated with defects/distortion in nanotubes and its ratio with G-peak estimates the quality of CNs, i.e., the higher is the G/D ratio, the higher is the quality. Since the low-frequency noise is usually associated with defects, the amplitude of the defect-related D-peak and the ratio G/D are important for the noise analysis. Our preliminary study showed that device with a higher G/D ratio is characterized by the lower noise level.[26]

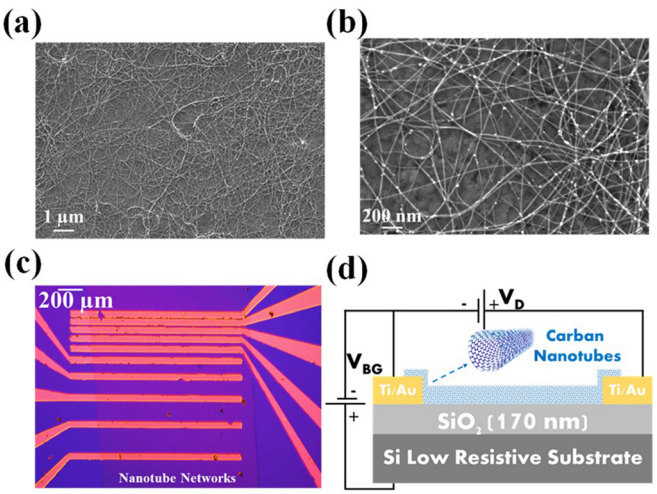

FIG. 1. (a) and (b) Scanning electron microscope images of the randomly oriented network of CNs at different magnifications. (c) Optical microscope image of the studied TLM structure. The Red leads represent the gold contacts deposited on oxidized Si before the transfer of nanotubes. The CNNs layer can be seen as a slightly darker area. (d) Schematic representation of the back-gated CNNs field-effect transistor along with the DC voltage biasing sources V_{BG} and V_D.

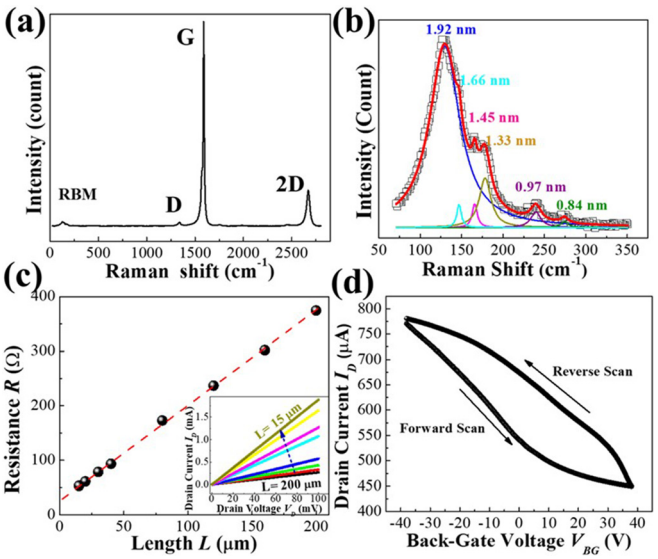

FIG. 2. (a) Raman spectra of the studied CNNs over a wide spectral range. (b) Zoom-in view of the RBM peak along with the Lorentzian peak fitting to estimate the diameter of nanotubes. (c) DC resistance as a function of device length. The red-dashed line indicates a linear approximation of the data points. Inset shows the current–voltage characteristics of the same devices. (d) The transfer current–voltage characteristics for one of the representative transistors.

Graphitic G-peak is attributed to the covalent bonds between carbon atoms, whereas RBM peak is associated with the coherent vibration of carbon atoms in the radial direction and exclusively appears only for CNs. It also allows estimating the diameter of a nanotube via equation $d_{CNTs} = \frac{A}{\omega_{RBM} - B}$, where d_{CNTs} is the diameter of nanotubes, $A = 217.8\,\mathrm{cm}^{-1}$, $B = 15.7\,\mathrm{cm}^{-1}$, and ω_{RBM} is the center frequency of the peak (in cm^{-1}).[26,29,31] The decomposition of Raman RBM peak along with the Lorentzian curves is shown in Fig. 2(b). These results identify the existence of different diameters of nanotubes ranging from 0.84 to 1.92 nm. Overall, Raman analysis indicated the typical characteristics of the studied CNNs.[27,28]

Figure 2(c) shows the resistance of CNNs as a function of device length. Each data point corresponds to the resistance of nanotubes devices of the given length. The red-dashed line indicates a linear approximation of data points, and its intersection with the Y-axis (i.e., at $L = 0\,\mu$m) yields the total contact resistance. In all studied devices, the contribution of contact resistance into total device resistance was relatively small. The current–voltage characteristics of the same devices are shown in the inset of Fig. 2(c).

Figure 2(d) shows the transfer current–voltage characteristic of one of the studied nanotube transistors. As seen, this back-gate transistor acts as a p-channel field effect transistor. The forward and reverse scans of back-gate voltage V_{BG} reveal significant hysteresis, which arises due to the deep trap levels in the active conducting layer and is typical for CNNs-based field-effect transistors. The characteristic time of the drain current drift is within the range from a few seconds to a few tens of minutes at fixed back-gate voltage V_{BG}.

Contrary to the DC electrical properties, noise properties varied significantly from device to device. This is a well-known phenomenon,[19,26,32] which specifies the high sensitivity of flicker noise to the structural quality of a sample. Particularly, noise measurements as a function of the back-gate voltage showed that although current always decreased with the increase in the V_{BG} value, the dependences of noise on V_{BG} varied between the tested devices. The noise spectra at different back-gate voltages for the exemplary as-fabricated device are shown in Fig. 3(a). Figure 3(b) shows the normalized drain current spectral noise density S_I/I^2 dependences at frequency $f = 10$ Hz on V_{BG} for the same device. The noise increases with a back-gate voltage for this particular device. It is seen that the noise spectra look like $1/f^{\gamma}$ noise with exponent γ increasing with the back-gate voltage [Fig. 3(a)].

The dependence of the exponent γ on V_{BG} is shown in Fig. 3(c). Since the spectrum is not a straight line in the log–log scale, the parameter γ was estimated for the frequency range from 1 to 10 Hz.

The noise properties of another representative as-fabricated device are shown in Fig. 4. Noise spectra at different back-gate voltages are shown in Fig. 4(a). The dependences of S_I/I^2 (at $f = 10$ Hz) and exponent γ on V_{BG} are shown in Figs. 4(b) and 4(c), respectively. Contrary to Figs. 3(b)–3(c), the dependences of noise and exponent γ on V_{BG} demonstrate maximum, which appear approximately at the same V_{BG}. This signifies the sensitivity of flicker noise, which varies between the specimens from the same batch owing to different concentrations of the trap levels. For both devices (in Figs. 3 and 4), the maximum value of the frequency exponent is close to $\gamma = 2$.

The low-frequency noise in semiconductor devices is often a superposition of generation-recombination (GR) and $1/f$ noise components,[33]

$$\frac{S_I}{I^2} = \frac{4N_t}{p^2 V}\frac{\tau F(1-F)}{\left(1+(2\pi f\tau)^2\right)} + \frac{A}{f}, \tag{1}$$

where N_t and F are the concentration and occupancy of traps responsible for GR noise, respectively, p is the concentration of free carriers (holes in studied devices), V is the volume of semiconductor, τ is the characteristic time constant associated with the return to equilibrium of the trap occupancy, and A is the amplitude of $1/f$ noise. The time constant τ can be expressed as $\tau = \tau_c F$, where τ_c is the capture time constant.[33] The first term in Eq. (1) represents the GR (Lorentzian) noise with the characteristic spectrum shape and time constant τ. At low frequencies $f_{char} \ll (2\pi\tau)^{-1}$, noise does not depend on the frequency and has a maximum at $F \cong 0.66$, i.e., when the Fermi level is slightly below the trap level responsible for GR noise in a p-channel transistor. At high frequencies, noise decreases as $1/f^2$. The superposition of GR and $1/f$ noise can provide a variety of the noise spectra shapes. We speculate that the observed noise power spectra in the studied CNNs devices are the superposition of $1/f$ noise and GR noise with a characteristic frequency $f_{char} < 1$ Hz. As follows from Eq. (1), the condition for the local maximum of noise satisfies the following equation:

$$2 - 3F - (2\pi f\tau_c)^2 F^3 = 0, \tag{2}$$

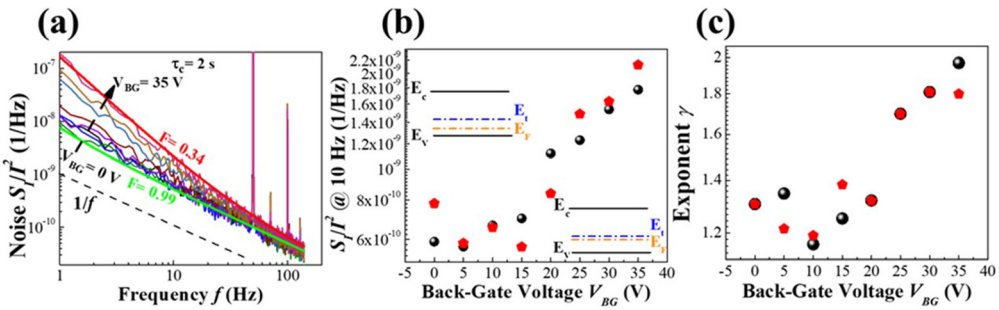

FIG. 3. (a) Normalized noise power spectra of CNNs back-gated transistor at different back-gate voltages V_{BG}. Smooth lines show the result of the fitting using Eq. (1) for two values of V_{BG} (0 V, 35 V). (b) Normalized noise power spectral density S_I/I^2 at frequency $f = 10$ Hz for the same specimen vs V_{BG}. Insets show the qualitative band diagrams with relative positions of the Fermi level E_F and trap level E_t, responsible for GR noise at different V_{BG}. (c) The dependence of exponent γ on V_{BG}. Different symbols correspond to two consecutive measurements with a time interval of 5 min.

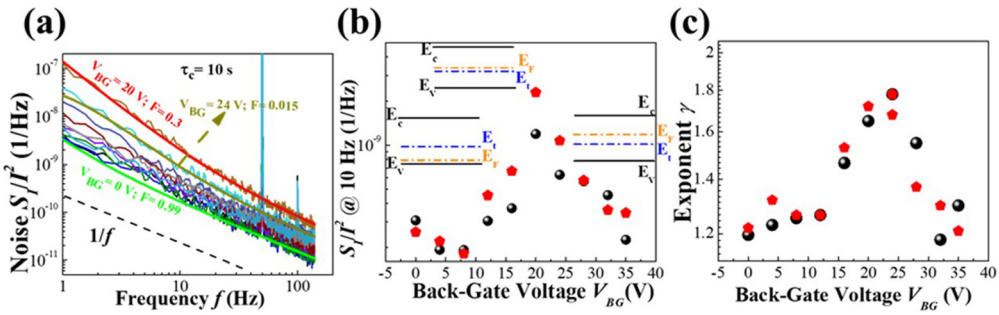

FIG. 4. (a) Normalized noise power spectra of another CNNs back-gated transistor at different back-gate voltages V_{BG}. Smooth lines show the results of the fitting using Eq. (1) for three values of V_{BG} (0, 20, and 24 V). (b) Normalized noise power spectrum S_I/I^2 at frequency $f = 10$ Hz for the same specimen vs V_{BG}. Insets show the qualitative band diagrams with relative positions of the Fermi level E_F and trap level E_t, responsible for GR noise at different voltages V_{BG} used for noise spectra fitting in (a). (c) The dependence of exponent γ on V_{BG}. Different symbols correspond to two consecutive measurements with a time interval of 5 min.

which is derived by differentiation of Eq. (1) and compared to zero. Analysis of Eq. (2) shows that at high frequencies, the maximum of noise corresponds to the Fermi level close or somewhat above the trap level in p-type material, i.e., $F < 0.66$.

Solid lines in Figs. 3(a) and 4(a) approximate a few power spectra lines using Eq. (1). The estimated characteristic time constants for these two devices are $\tau_c = 2$ s [Fig. 3(a)] and $\tau_c = 10$ s [Fig. 4(a)]. It is important that the fits were done for the same values of N_t and τ_c for each sample. In the fitting procedure, only the occupancy function F and the amplitude of $1/f$ noise were adjusted. The band diagrams in the insets in Figs. 3(b) and 4(b) schematically illustrate the positions of the Fermi level E_F, which correspond to the occupancy function F of the energy trap level E_t, used in the fitting procedure. We can conclude that different GR noise properties for the studied samples are caused by variations in concentrations and energy positions of the deep level traps, characterized by the frequencies $f_{char} = (2\pi\tau)^{-1}$ below 1 Hz. The trap concentration can be high enough to affect the Fermi level position. Even a higher spread of GR noise components between the tested devices can be present in such a case. These results show that contrary to the majority of publications where just $1/f$ noise was observed, studied devices demonstrate significant contribution of the GR noise. This is an indication that just one kind of traps dominates the noise properties, and the concentration of all other traps (defects) is small.

It was found that keeping the CNNs devices in the ambient atmosphere of laboratory air (45% relative humidity) leads to a slow decrease in the DC resistance, observed even in a relatively short time [Fig. 5(a)]. Exposure to synthetic air partially restores the DC resistance and makes it more stable over time. Therefore, we conclude that humidity is the main reason behind the DC resistance drift. Interestingly, noise decreased when CNNs transistors were exposed to the atmosphere of laboratory air. Figure 5(b) shows the noise power spectral densities for the same device as in Fig. 3, after keeping it in the ambient atmosphere for about a month and after exposure to synthetic air. It can be seen that an ambient atmosphere decreases low-frequency noise and reduces the GR noise component. Even a short time exposure to synthetic air increases the noise amplitude and spectrum slope, which indicates an increase in both $1/f$ and GR components of noise. This phenomenon is not common for low-dimensional systems. It was shown elsewhere that exposure to the atmosphere increases the noise,[34] and keeping devices in vacuum or surface protection reduces the noise of low-dimensional devices.[35–41]

The reported experimental studies of the ambient atmosphere effect on noise in CNs are limited and contradictory. While in Ref. 20, the authors observed substantial enhancement of noise in studied devices, others reported the decrease in noise in a single nanotube transistor owing to exposure of devices to the ambient atmosphere.[42] In our study, noise decreased as a result of exposure to laboratory air. This is an unusual and unexpected behavior because in the majority of cases, contamination leads to noise increase. We can speculate that adsorbed water molecules p-doped the nanotubes, which, in turn, reduced their DC resistance. According to Eq. (1), an increase in hole's concentration, p, decreases the amplitude of GR noise as $1/p^2$. It also shifts the Fermi level closer to the valence band. This, in turn, increases the occupancy function F, making GR noise even less intense. Even short exposure to synthetic air induces water molecules desorption, which, in turn, decreases the hole's concentration and increases the GR noise component. The sensitivity of the resistance and especially the noise spectra to the environment makes CNNs promising as gas sensing devices. While resistance changes within ~1%, the change in noise amplitude at low frequencies is about an order of magnitude [see Fig. 5(b)]. Furthermore, change in the noise spectra shape has potential for selective gas sensing. Similar approach for selective gas sensing was previously proposed,[43] and later confirmed for exfoliated graphene

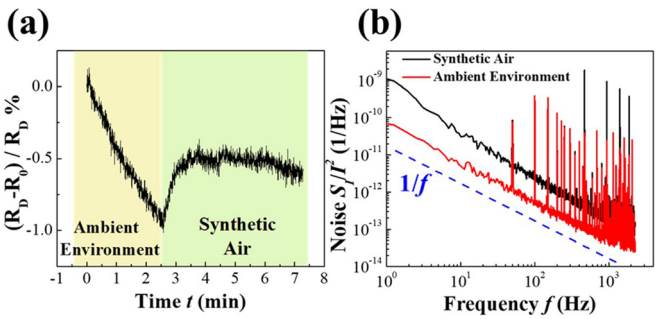

FIG. 5. (a) Relative change of the DC resistance of CNNs transistor as a function of time under the ambient atmosphere of laboratory air and next in synthetic air, introduced at time $t = 2.5$ min. (b) Noise power spectral density observed in the studied device as presented in Fig. 3 after a month of exposure to laboratory air and just after introducing the synthetic air.

devices.[44] In comparison with graphene, CNNs devices have advantages of fabrication simplicity, scalability, and potentially low price.

In conclusion, we observed that the low-frequency noise in CNNs transistors is not a pure 1/*f* noise but rather a superposition of 1/*f* and generation-recombination noise. The generation-recombination noise component was caused by the traps of the energy level close to or somewhat below the Fermi level in a *p*-channel CNNs field-effect transistors, characterized by a time constant range from 2 to 10 s. Such long relaxation processes also contribute to the observed hysteresis of the DC resistance upon sweeping the back-gate voltage. Although the DC characteristics of the studied devices were identical, GR noise and their dependence on back-gate voltage were different owing to variations in trap distribution responsible for the noise. The unusual effect of the noise reduction as a result of aging was explained by the *p*-doping of nanotubes in the environment of humid laboratory air. Our study confirmed the environment-dependent noise properties of CNNs transistors, and such effects need to be taken into account in the development of carbon nanotube-based selective gas sensing devices.

The work was supported by the National Science Centre, Poland, Research Project No. 2019/35/B/ST7/02370 "System of gas detection by two-dimensional materials," and the Foundation for Polish Science through TEAM Project No. POIR.04.04.00-00-3D76/16 (TEAM/2016-3/25). This study was also partially supported by CENTERA Laboratories in the frame of the International Research Agendas program for the Foundation for Polish Sciences, co-financed by the European Union under the European Regional Development Fund (No. MAB/2018/9).

DATA AVAILABILITY

The data that support the findings of this study are available from the corresponding author upon reasonable request.

REFERENCES

[1]S. H. Chae and Y. H. Lee, "Carbon nanotubes and graphene towards soft electronics," Nano Convergence **1**, 15 (2014).
[2]J. Tang, Q. Cao, G. Tulevski, K. A. Jenkins, L. Nela, D. B. Farmer, and S.-J. Han, Nat. Electron. **1**(3), 191 (2018).
[3]W. Zhu, T. Low, H. Wang, P. Ye, and X. Duan, 2D Mater. **6**(3), 032004 (2019).
[4]J. Hou, H. Zhang, Y. Hu, X. Li, X. Chen, S. Kim, Y. Wang, G. P. Simon, and H. Wang, ACS Appl. Mater. Interfaces **10**(23), 20182 (2018).
[5]Y. Wang and J. T. Yeow, J. Sens. **2009**, 493904.
[6]Y. Zhou and R. Azumi, Sci. Technol. Adv. Mater. **17**(1), 493 (2016).
[7]S. Park, M. Vosguerichian, and Z. Bao, Nanoscale **5**(5), 1727 (2013).
[8]A. Saha, C. Jiang, and A. A. Martí, Carbon **79**, 1 (2014).
[9]Y. Cao, S. Cong, X. Cao, F. Wu, Q. Liu, M. R. Amer, and C. Zhou, Top. Curr. Chem. **375**, 75 (2017).
[10]X. He, N. Fujimura, J. Meagan Lloyd, K. J. Erickson, A. Alec Talin, Q. Zhang, W. Gao, Q. Jiang, Y. Kawano, and R. H. Hauge, Nano Lett. **14**(7), 3953 (2014).
[11]N. Titova, I. A. Gayduchenko, M. V. Moskotin, G. F. Fedorov, and G. N. Goltsman, "Carbon nanotube based terahertz radiation detectors," J. Phys.: Conf. Ser. **1410**, 012208 (2019).
[12]R. Wang, L. Xie, S. Hameed, C. Wang, and Y. Ying, Carbon **132**, 42 (2018).
[13]D. Suzuki, Y. Ochiai, and Y. Kawano, ACS Omega **3**(3), 3540 (2018).
[14]T. Tanaka and E. Sano, Jpn. J. Appl. Phys., Part 1 **53**(9), 090302 (2014).
[15]C. Barone, G. Landi, C. Mauro, S. Pagano, and H. C. Neitzert, Diamond Relat. Mater. **65**, 32 (2016).
[16]E. Sano and T. Tanaka, J. Appl. Phys. **115**(15), 154507 (2014).
[17]M.-K. Joo, M. Mouis, D.-Y. Jeon, G.-T. Kim, U. J. Kim, and G. Ghibaudo, J. Appl. Phys. **114**(15), 154503 (2013).
[18]P. G. Collins, M. S. Fuhrer, and A. Zettl, Appl. Phys. Lett. **76**(7), 894 (2000).
[19]E. S. Snow, J. P. Novak, M. D. Lay, and F. K. Perkins, Appl. Phys. Lett. **85**(18), 4172 (2004).
[20]F. Liu, K. L. Wang, D. Zhang, and C. Zhou, Appl. Phys. Lett. **89**(6), 063116 (2006).
[21]A. Behnam, G. Bosman, and A. Ural, in 2009 Device Research Conference (2009).
[22]V. A. Sydoruk, M. V. Petrychuk, A. Ural, G. Bosman, A. Offenhäusser, and S. A. Vitusevich, Carbon **53**, 252 (2013).
[23]A. Setiadi, H. Fujii, S. Kasai, K.-I. Yamashita, T. Ogawa, T. Ikuta, Y. Kanai, K. Matsumoto, Y. Kuwahara, and M. Akai-Kasaya, Nanoscale **9**(30), 10674 (2017).
[24]I. V. Anoshkin, A. G. Nasibulin, Y. Tian, B. Liu, H. Jiang, and E. I. Kauppinen, Carbon **78**, 130 (2014).
[25]S. Smirnov, I. V. Anoshkin, P. Demchenko, D. Gomon, D. V. Lioubtchenko, M. Khodzitsky, and J. Oberhammer, Nanoscale **10**(26), 12291 (2018).
[26]A. Rehman, S. Smirnov, A. Krajewska, D. B. But, M. Liszewska, B. Bartosewicz, K. Pavlov, G. Cywinski, D. Lioubtchenko, and W. Knap, Mater. Res. Bull. **134**, 111093 (2021).
[27]A. Jorio and R. Saito, J. Appl. Phys. **129**(2), 021102 (2021).
[28]M. S. Dresselhaus, G. Dresselhaus, R. Saito, and A. Jorio, Phys. Rep. **409**(2), 47 (2005).
[29]P. T. Araujo, S. K. Doorn, S. Kilina, S. Tretiak, E. Einarsson, S. Maruyama, H. Chacham, M. A. Pimenta, and A. Jorio, Phys. Rev. Lett. **98**(6), 067401 (2007).
[30]R. Jackson and S. Graham, Appl. Phys. Lett. **94**(1), 012109 (2009).
[31]S. Smirnov, I. V. Anoshkin, A. Generalov, D. V. Lioubtchenko, and J. Oberhammer, RSC Adv. **9**(26), 14677 (2019).
[32]A. A. Balandin, *Noise and Fluctuations Control in Electronic Devices* (American Scientific Publishers, 2002).
[33]M. E. Levinshtein and S. L. Rumyantsev, Semicond. Sci. Technol. **9**(6), 1183 (1994).
[34]J. Renteria, R. Samnakay, S. L. Rumyantsev, C. Jiang, P. Goli, M. S. Shur, and A. A. Balandin, Appl. Phys. Lett. **104**(15), 153104 (2014).
[35]J.-W. Wang, Y.-P. Liu, P.-H. Chen, M.-H. Chuang, A. Pezeshki, D.-C. Ling, J.-C. Chen, Y.-F. Chen, and Y.-H. Lee, Adv. Electron. Mater. **4**(1), 1700340 (2018).
[36]G. Liu, S. L. Rumyantsev, C. Jiang, M. S. Shur, and A. A. Balandin, IEEE Electron Device Lett. **36**(11), 1202 (2015).
[37]C.-K. Kim, C. H. Yu, J. Hur, H. Bae, S.-B. Jeon, H. Park, Y. M. Kim, K. C. Choi, Y.-K. Choi, and S.-Y. Choi, 2D Mater. **3**(1), 015007 (2016).
[38]D. Sharma, M. Amani, A. Motayed, P. B. Shah, A. Glen Birdwell, S. Najmaei, P. M. Ajayan, J. Lou, M. Dubey, and Q. Li, Nanotechnology **25**(15), 155702 (2014).
[39]X. Xie, D. Sarkar, W. Liu, J. Kang, O. Marinov, M. Jamal Deen, and K. Banerjee, ACS Nano **8**(6), 5633 (2014).
[40]S. Ghatak, S. Mukherjee, M. Jain, D. D. Sarma, and A. Ghosh, APL Mater. **2**(9), 092515 (2014).
[41]V. K. Sangwan, H. N. Arnold, D. Jariwala, T. J. Marks, L. J. Lauhon, and M. C. Hersam, Nano Lett. **13**(9), 4351 (2013).
[42]M. Ishigami, J. H. Chen, E. D. Williams, D. Tobias, Y. F. Chen, and M. S. Fuhrer, Appl. Phys. Lett. **88**(20), 203116 (2006).
[43]S. Rumyantsev, G. Liu, M. S. Shur, R. A. Potyrailo, and A. A. Balandin, Nano Lett. **12**(5), 2294 (2012).
[44]K. R. Amin and A. Bid, Appl. Phys. Lett. **106**(18), 183105 (2015).